Bull. Mater. Sci. (2021) 44:118
https://doi.org/10.1007/s12034-021-02380-y

Systematic effects of Ti doping on the electronic properties of $LaNiO_3$ thin films

SOURAV SINGH TOMAR#, EKTA YADAV#, KAVITA SONI and K R MAVANI*
Discipline of Physics, Indian Institute of Technology (IIT) Indore, Indore 453 552, India
*Author for correspondence (krushna@iiti.ac.in)
#These authors contributed equally to this article.

MS received 25 June 2020; accepted 14 November 2020

Abstract. We have deposited a series of $LaNi_{1-x}Ti_xO_3$ (x = 0–0.10) thin films on $LaAlO_3$ (001) (LAO) single-crystal substrates using pulsed laser deposition (PLD) method and studied the effect of Ti doping on the structural and electronic properties. All the films are highly oriented towards the substrate (001) axis. The incorporation of Ti ions in $LaNiO_3$ system causes an increase in the compressive strain. The temperature-dependent resistivity curves indicate that the films remain metallic even at low-temperature range. In spite of a lower percentage of variation in Ti doping, the overall resistivity of the system increases quite systematically with increase in Ti content. The power-law fitting of resistivity data show the non-Fermi behaviour of the system. Besides, a systematic blue shift of Raman modes is observed with increase in doping, which indicates a change in Ni–O–Ni bond angle and NiO_6 octahedra distortion due to Ti doping in $LaNiO_3$ thin films. The temperature-dependent Raman spectra show the red shift with increase in temperature in all the thin films. The observed systematic variations in resistivity and Raman modes both originated due to Ti doping in the system.

Keywords. Rare-earth nickelates; epitaxial strain; metal–insulator transition; Raman spectroscopy.

1. Introduction

The perovskite nickelates having chemical formula $RNiO_3$ (R = rare-earth ion) show first-order metal to insulator transition and have many applications in the field of ultra-fast switching, optical electronics, fuel cells, gas sensing, etc. [1–4]. In $RNiO_3$ family, $LaNiO_3$ (LNO) shows paramagnetic-metallic state throughout the temperature range (12–300 K) and does not show any metal to insulator transition. On the other hand, other $RNiO_3$ compounds show metal to insulator transition with temperature [3,4]. In bulk, it is difficult to synthesis LNO in single-phase form [5], but with the advancement of thin-film deposition techniques, thin films can be synthesized easily. The electronic properties of LNO can be tuned by varying strain, doping, thickness, etc. [6].

The LNO thin films have a wide range of applications in electrode devices, thermal and gas sensors and switches [7]. It is highly used in oxide electronic device applications because of its highly conductive nature. The electronic transport of LNO depends on the overlapping between nickel (Ni) 3d and oxygen 2p orbitals, which is very sensitive on the Ni–O–Ni bond angle. Other factors like doping, pressure, strain affects the Ni–O–Ni bond angle and charge carrier density, which results in tuning the electronic behaviour [8,9].

Doping acts as a controlling parameter of electronic transport in strongly correlated oxides by altering the carrier concentration. Carrier concentration can be changed either by doping of divalent Sr, trivalent Nd, tetravalent Th ion at trivalent La-sites [10,11] or doping of Mn, Fe, Cu, Zn, Mo, Ti and W at Ni sites [12–14]. For titanium (Ti), the most stable oxidation state is 4+ in its oxide form. Doping of Ti ion at trivalent Ni sites can change valence state of Ni. As Ti^{4+} has no electron in its 3d band, so by replacing Ni with less electronically active Ti ion, we can drive the system towards the insulating state. To study the doping effect of Ti, we have synthesized $LaNi_{1-x}Ti_x$ (x = 0–0.10) thin films on $LaAlO_3$ (LAO) single-crystal substrate having a thickness of 8 nm. After synthesis, the structural, vibrational and electronic properties of thin films have been studied.

2. Experimental

The thin films of $LaNi_{1-x}Ti_xO_3$ (x = 0–0.10) (LNTO) were deposited on LAO (001) single-crystal substrate by pulsed laser deposition (PLD) method. The pellets used to make the thin films were prepared using solid-state reaction method. The pellets were sintered at 1000°C. KrF excimer laser (λ = 248 nm) was used for the deposition of thin films, and its energy was set at 310 mJ. Thin films of

Published online: 28 April 2021

$LaNi_{1-x}Ti_xO_3$ (x = 0–0.10) were prepared at the substrate temperature of 720°C and oxygen partial pressure of 40 Pa. Just after deposition, all the thin films were *in-situ* annealed at 1000 Pa oxygen pressure for 3 min to maintain oxygen stoichiometry. The distance between target and substrate was 4 cm, and the repetition rate of the laser pulse was 4 Hz. The thickness of the films was 8 nm approximately. The purity and structural orientation of the thin films was studied using X-ray diffraction (XRD) measurement using PanAlytical made set up. The temperature-dependent resistivity measurements of thin films were performed using the four-probe method in a Janis Research made closed cycle refrigerator (CCR) cryostat. For the measurements, Keithley-made source and measurement station (model no.: 2612A) was used. The range of temperature to measure resistance was 12–300 K. Vibrational modes analysis of thin films was done using LABRAM micro-Raman spectrometer with 632.8 nm wavelength of the laser. At room temperature, ×100 lens was used to collect Raman scattered signals while ×50 lens was used to collect Raman scattered signals in temperature-dependent Raman spectroscopy. Liquid N_2 was used as a coolant, and temperature range of measurement was 93–300 K.

3. Results and discussion

In order to check phase purity of the prepared thin films, XRD measurements have been carried out. Figure 1a and b shows the full-scale XRD pattern and enlarged view of the (002) Bragg's diffraction of $LaNi_{1-x}Ti_xO_3$ (x = 0–0.10) (LNTO) thin films, respectively. It can be seen from figure 1a that all the films are pure and grown in the same direction of substrate LAO (001). The pseudo-cubic lattice parameter of $LaNiO_3$ is 3.837 Å and that of LAO is 3.789 Å, the lattice mismatch is approximately –1.26%; thus the film tries to compress itself, which results in an increase of out-of-plane lattice parameter. Figure 1b shows the shift of Bragg's peak towards low 2θ value with increase in Ti doping. It is clear from figure 1b that all the Ti-doped LNO films experience compressive strain on $LaAlO_3$ substrate as they lie in the lower 2θ side as compared to the substrate. In addition, there is a systematic shift in XRD peak positions representing (002) plane with Ti-doping. From this XRD peak position, we have calculated the lattice parameters of these thin films using Bragg's relation. The calculated lattice parameters are tabulated in table 1.

It is clear from the table that the lattice parameters increase with increase in Ti-doping content. Using this, we have quantified the lattice mismatch for all the LNTO films using the formula:

$$\varepsilon(\%) = \frac{a_{\text{subs}} - a_{\text{film}}}{a_{\text{subs}}} \times 100,$$

where a_{subs} and a_{film} are the lattice parameters of substrate and thin film, respectively. The calculated value of lattice mismatch, proportional to strain, increase with increment in Ti-doping as shown in table 1. It suggests that the extent of compressive strain is increasing in $LaNiO_3$ thin films with incorporation of Ti doping.

The electronic transport of the Ti-doped $LaNiO_3$ thin films has been studied by temperature-dependent resistivity measurement. The corresponding resistivity *vs.* temperature plots of $LaNi_{1-x}Ti_xO_3$ (x = 0–0.10) thin films are shown in figure 2. It is clear from the figure that all the films remain metallic below room temperature and the overall resistivity increase with Ti-doping systematically. As the most stable oxidation state of Ti is tetravalent (4+), so doping of Ti in the $LaNiO_3$ system having Ni^{3+} state can cause some changes in the electronic state of the system. This may result in a reduction in the charge transfer between Ni^{3+}–O–Ni^{3+} pairs, thereby

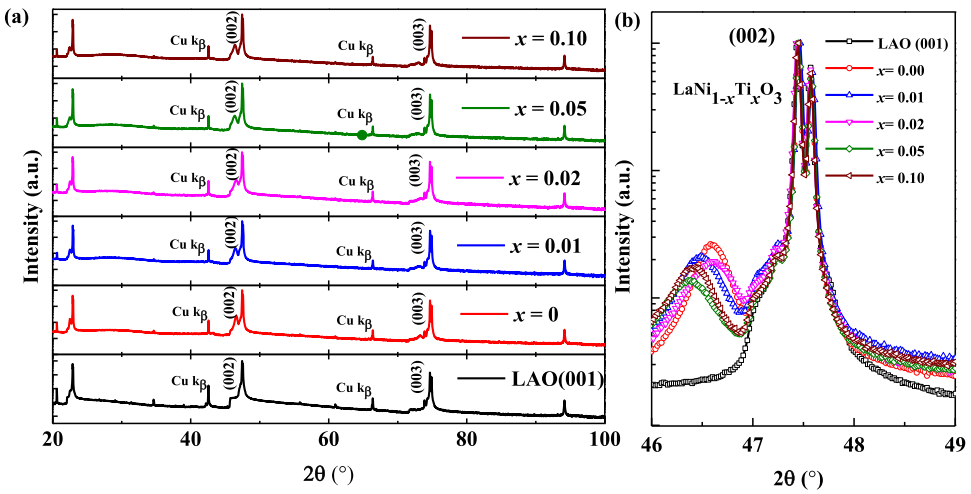

Figure 1. (**a**) X-ray diffraction patterns of $LaNi_{1-x}Ti_xO_3$ (x = 0–0.10) thin films grown on LAO (001) substrate. (**b**) Enlarged view of (002) Bragg's diffraction of $LaNi_{1-x}Ti_xO_3$ (x = 0–0.10) thin films.

Table 1. XRD peak positions, lattice parameters and lattice mismatch of $LaNi_{1-x}Ti_xO_3$ (x = 0–0.10) thin films.

x	2θ (°)	Lattice parameter (Å)	Lattice mismatch (%)
0	46.582	3.898	–2.84
0.01	46.48	3.902	–2.94
0.02	46.52	3.901	–2.92
0.05	46.42	3.908	–3.11
0.10	46.380	3.91	–3.16

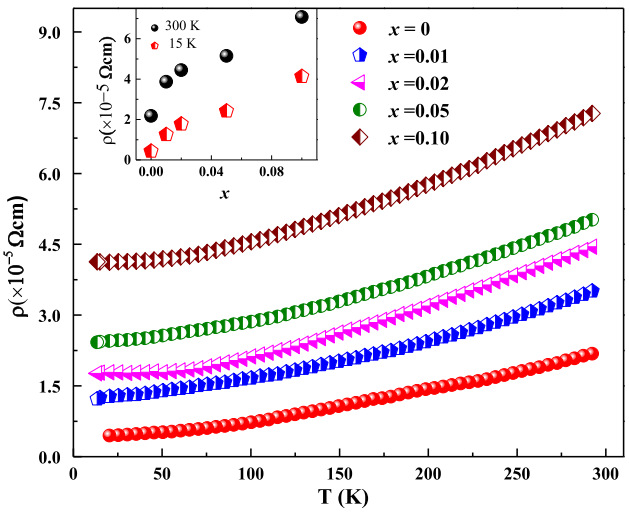

Figure 2. Resistivity *vs.* temperature plots for $LaNi_{1-x}Ti_xO_3$ (x = 0–0.10) thin films on LAO (001). The inset figure shows resistivity *vs.* doping plot at room temperature, i.e., 300 and 15 K.

causing weak localization of the charge carriers and an increase in resistivity with Ti-doping [15]. Earlier, it was reported that the $LaNiO_3$ remain metallic throughout the temperature range without any metal to insulator transition [3,4]. Figure 2 shows that the resistivity of the system increases with increase in doping amount of Ti. The resistivity at 15 and 300 K also indicate the same trend. There is no metal to insulator transition observed in the system. However, at low temperature, a flat curve is observed; this means that the Ti doping is suppressing the metallic state. At a larger amount of Ti doping, it may introduce metal to insulator transition.

Power-law equation $\rho_{NFL}(T) = \rho_0 + AT^n$ is used to fit the resistivity curves, here $n < 2$, ρ_0 is residual resistivity (resistivity at absolute zero), A is a constant that represents the electron–electron scattering strength [16]. For $n = 2$, compound falls in the category of Landau Fermi liquid, and $n <$ 2 indicates the deviation from this classical behaviour [17,18]. The parameter n is adjustable and n = 1.6 and 1.3 are obtained from the fittings of power-law equation indicating the persistence of non-Fermi liquid (NFL) behaviour. Figure 3 shows the fitting of the curves with power law equation, and the fitted parameters are shown in table 2. It is clear from the table that for the undoped LNO film, n = 1.3,

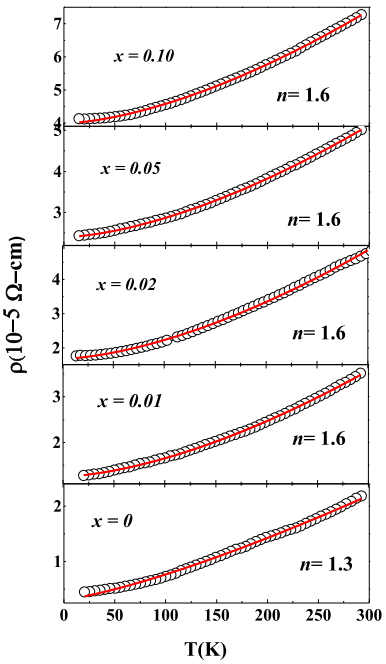

Figure 3. Resistivity *vs.* temperature plots for $LaNi_{1-x}Ti_xO_3$ (x = 0–0.10) thin films on LAO (001). The red line shows the fitting of resistivity using the power law equation.

Table 2. Transport properties of $LaNi_{1-x}Ti_xO_3$ (x = 0–0.10) thin films deposited on LAO.

x	n	A ($\times 10^{-9}$) (Ω cm $(K^n)^{-1}$)	ρ_0 ($\times 10^{-5}$) (Ω cm)
0	1.3	11.32 ± 0.07	0.32 ± 0.01
0.01	1.6	2.51 ± 0.01	1.26 ± 0.01
0.02	1.6	3.44 ± 0.02	1.68 ± 0.01
0.05	1.6	2.96 ± 0.01	2.40 ± 0.01
0.10	1.6	3.71 ± 0.01	3.99 ± 0.01

i.e., NFL behaviour is observed, while all the other LNTO films show the NFL behaviour with n = 1.6. Also, residual resistivity i.e., ρ_0 increases with increase in Ti-doping, as shown in table 2. This may be due to disorder induced in the system due to Ti-doping.

Raman spectroscopy was used to investigate the vibrational modes of thin films. The group theory gives five Raman active modes (A_{1g} and four E_g) for bulk $LaNiO_3$ [19–22]. In our case, we observed two modes A_{1g} and E_g. The A_{1g} mode describes the rotations of NiO_6 about the trigonal axis [111], which is directly related to the octahedral tilt angle, and the E_g modes describe the bending of the Ni–O bond [21]. Earlier, it has been reported that A_{1g} and E_g modes for a thin film of LNO on single-crystal LAO are observed at 214 and 403 cm^{-1}, respectively [19]. In the present study, A_{1g} and E_g (bending of Ni–O bond) modes for the parent LNO are observed nearly at 196 and 402.5 cm^{-1}, respectively, as shown in figure 4a. It is observed that

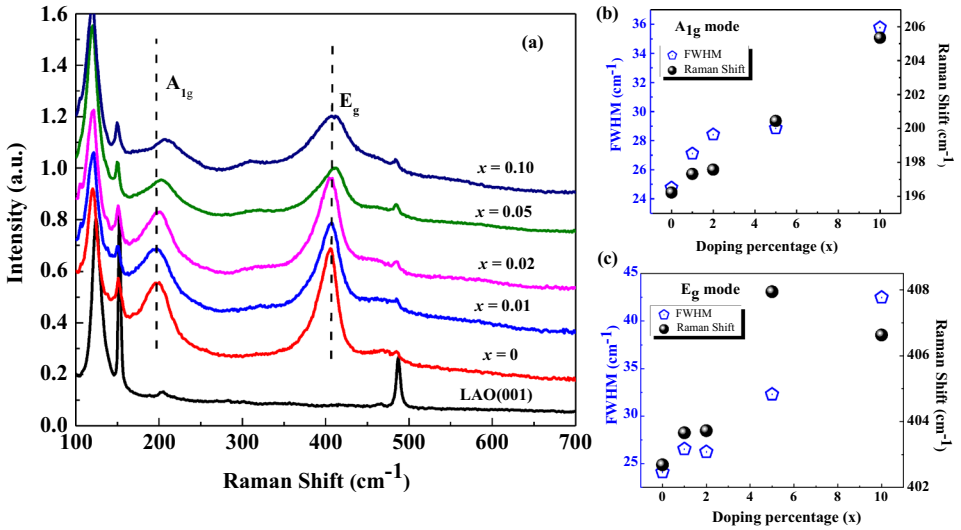

Figure 4. (**a**) Room-temperature Raman spectra of $LaNi_{1-x}Ti_xO_3$ (x = 0–0.10) thin films. (**b**) The variation of Raman FWHM and peak position of A_{1g} and E_g Raman modes with Ti doping percentage in $LaNi_{1-x}Ti_xO_3$ (x = 0–0.10) thin films.

both the A_{1g} and E_g modes are blue-shifted by increasing Ti doping percentage, but in case of E_g mode the Raman shift is not systematic as shown in figure 4b. Earlier reports suggested that the shifting of A_{1g} mode is –23 cm^{-1} per degree shift in NiO_6 octahedral angle [20,23]. Therefore, by increasing the doping of Ti from 0 to 10%, the shift in A_{1g} mode is nearly 13 cm^{-1}. If this shift is converted into the tilt in Ni–O–Ni octahedral angle, then it nearly equals to 0.56° with respect to the undoped film. Moreover, broadening of Raman modes is quantified by calculating FWHM (full-width at half-maximum) of the Raman modes. It was observed that there is broadening of A_{1g} and E_g modes with the increase of Ti doping in the system, as shown in table 3. This broadening is more pronounced for A_{1g} mode.

At this point, it should be noted that Raman scattering has a potential to probe the presence of compressive/tensile strain in the sample. The presence of compressive or tensile strain would result to shift in the position of Raman mode towards higher wavenumber side (blue shift) and lower wavenumber side (red shift), respectively [22,24]. In the present investigations, the shifting of Raman modes towards higher wavenumber with Ti-doping is clearly visible in figure 4. This infers that compressive strain is increasing in the material with Ti-doping, and this strain is responsible for the increase in resistivity. This is also consistent with the increase in lattice mismatch-induced strain calculated from XRD patterns.

To study the effects of temperature variations on the Raman modes, we performed the Raman measurements in the temperature range of 93–300 K for all the samples and shown in figure 5. Both the Raman modes A_{1g} and E_g are affected by the change in temperature, although neither disappears. The A_{1g} mode is red-shifted in all the systems with an increase in temperature. Such a shift indicates the influence of temperature on the rotation of NiO_6 octahedra. The E_g mode is also showing red shift (not as large as A_{1g} mode) for all the films with an increase in temperature and suggests the bending of Ni–O–Ni bond. It is well known that with increase in temperature, there is thermal expansion and interatomic bond lengthening in the materials. As a result, the force constant changes and the Raman active vibrational modes undergo red shift with rise in temperature. This temperature-dependent red shift of Raman modes has already been observed for various perovskites oxides

Table 3. Fitting parameters of Raman FWHM and Raman shift position of $LaNi_{1-x}Ti_xO_3$ (x = 0–0.10) thin films.

	A_{1g} mode		E_g mode	
x	FWHM (cm^{-1})	Raman shift (cm^{-1})	FWHM (cm^{-1})	Raman shift (cm^{-1})
0	24.75 ± 1.29	196.22 ± 0.28	24.10 ± 1.10	402.68 ± 0.29
0.01	27.10 ± 1.43	197.57 ± 0.29	26.54 ± 0.88	403.66 ± 0.21
0.02	28.41 ± 1.58	197.32 ± 0.33	26.24 ± 0.83	403.72 ± 0.21
0.05	28.85 ± 1.64	200.47 ± 0.38	32.29 ± 1.19	407.94 ± 0.29
0.10	35.78 ± 1.84	205.34 ± 0.40	42.48 ± 0.87	406.62 ± 0.16

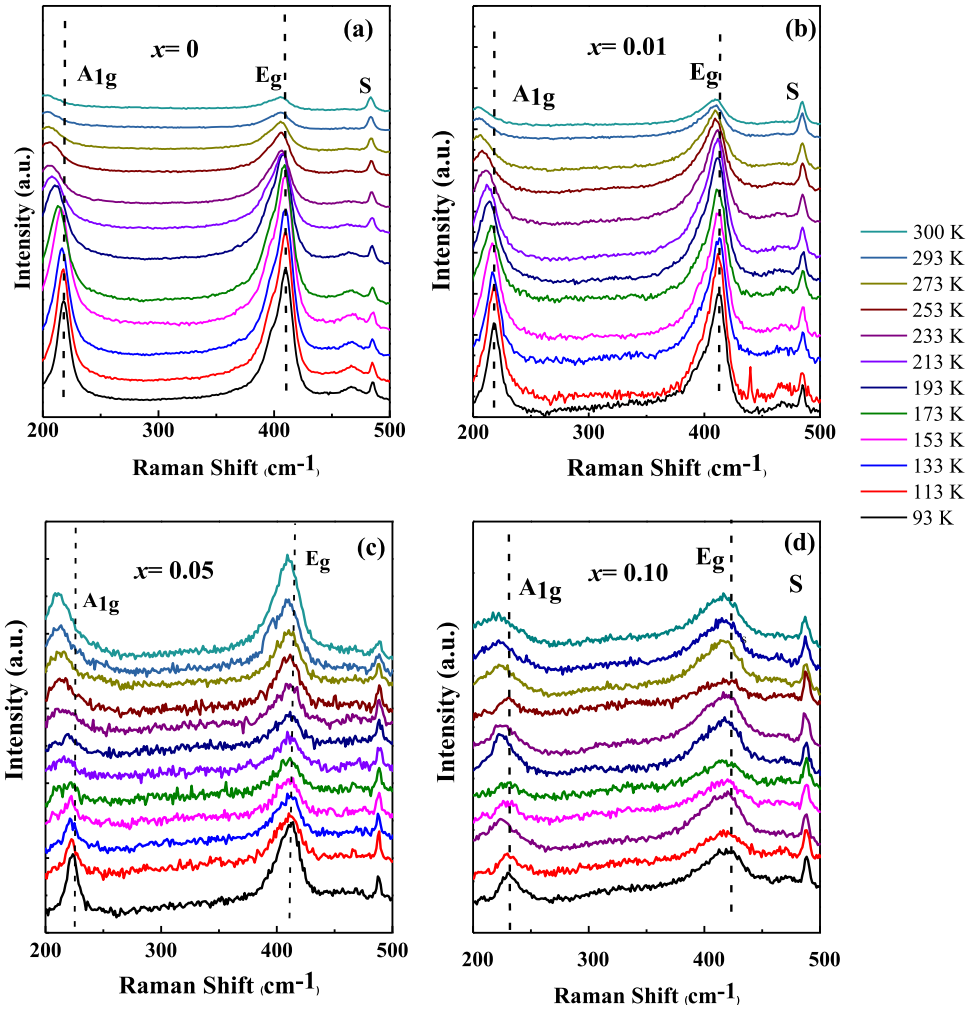

Figure 5. (**a–d**) Temperature-dependent Raman spectra of $LaNiO_3$, $LaNi_{0.99}Ti_{0.01}O_3$, $LaNi_{0.95}Ti_{0.05}O_3$ and $LaNi_{0.90}Ti_{0.10}O_3$ thin films, respectively.

also [19,20,23]. The red shift of Raman modes is also validated by the Balkanski model, in which the anharmonic contribution to the temperature dependence of the phonon position is given by [25]:

$$w(T) = w(0) - A\left[1 + \Sigma \frac{1}{\exp\left(\frac{h\omega_i}{2\pi kT}\right) - 1}\right],$$

where the term $w(0)$ is the Raman shift at 0° K, A (anharmonic coefficient) is the contribution from higher order terms for three phonon processes. With increase in temperature, the terms with the factor A scales systematically, which could be the main contributing factor for the red shift of the Raman modes with temperature.

There is a significant change in FWHM of A_{1g} and E_g modes observed with temperature. In all samples, the FWHM increases with increase in temperature as expected due to thermal broadening. However, the overall spectrum is maintained in all the films, and no drastic change occurs, which suggests $LaNiO_3$ does not go through any phase transition in the investigated temperature range.

4. Conclusion

We have studied the effects of moderate doping of Ti at Ni-site in $LaNiO_3$ thin films. Doping dependent systematic variations in the Raman modes and resistivity are found to be related. Systematic variations of doping on the structural and the electronic properties of $LaNi_{1-x}Ti_xO_3$ (x = 0–0.10) thin films deposited on single-crystal LAO substrate have been observed. XRD results suggest that incorporation of Ti ions in the system resulted in an increase in the lattice parameter as well as lattice mismatch-induced strain for LNTO thin films. The effect of doping suggested that the resistivity of the system increases with doping. The theoretical fitting of resistivity suggested that in large temperature range system persisted NFL behaviour. Raman spectra show a red shift and increase in Raman FWHM with Ti-doping, thereby highlighting a structural disorder induced in the system due to Ti-doping. Increase in bending and rotation of Ni–O–Ni bonds with the reduction in temperature have been observed in the temperature-dependent Raman spectra.

Acknowledgements

This study was supported through BRNS, India (project no.: 37(3)/14/28/2017-BRNS/37225) and SERB, India (project no.: EMR/2017/001821) of KRM. EY acknowledges CSIR, New Delhi, for providing fellowship through grant no. 1061751693. The facility of Raman Spectrometer under DST-FIST project no. SR/FST/PSI-225/2016 of Discipline of Physics, IIT Indore, is also acknowledged.

References

[1] Medarde M L 1997 *J. Phys.: Condens. Matter* **9** 1679
[2] Yang Z, Ko C and Ramanathan P 2011 *Annu. Rev. Mater. Res.* **41** 337
[3] Catalano S, Gibert M, Fowlie J, Iniguez J, Triscone J M and Kreisel J 2018 *Rep. Prog. Phys.* **81** 046501
[4] Catalan G 2008 *Phase Transit.* **81** 729
[5] Fowlie J 2019 *Thesis* Springer International Publishing
[6] Liu J, Kargarian M, Kareev, Gray B, Ryan P J, Cruz A *et al* 2013 *Nat. Commun.* **4** 2714
[7] Kyung Hwang D, Kim S, Lee J H, Hwang L S and Kim L D 2011 *J. Mater. Chem.* **21** 1959
[8] Torrence J B, Lacorre P, Nazzal A I, Ansaldo E J and Niedermayer C 1992 *Phys. Rev. B* **45** 8209
[9] Catalan G, Bowman R W and Gregg J M 1999 *J. Appl. Phys.* **87** 606
[10] Garcia-Munoz J L, Suaaidi M, Martinez-Lope M J and Alonso J A 1995 *Phys. Rev. B* **52** 13563
[11] Alonso J A, Matrinez-Lope M J and Hidalgo M A 1995 *J. Solid State Chem.* **116** 146
[12] Chandra M, Das S, Aziz F, Tripathi S and Mavani K R 2015 *Solid State Commun.* **219** 16
[13] Alvarez I, Veiga M L and Pico C 1998 *J. Solid State Chem.* **136** 313
[14] Yadav E, Harishankar S, Soni K and Mavani K R 2018 *Appl. Phys. A* **124** 614
[15] Chaitanya Lekshmi I, Gayen A, Sarma D D, Hegde M S, Chockalingam S P and Chandrasekhar N 2005 *J. Appl. Phys.* **98** 093527
[16] Wang L, Chang L, Yin X, Rusydi A, You L, Zhou Y *et al* 2017 *J. Phys.: Condensed Matter* **29** 025002
[17] Vucicevic J, Tanaskovic D, Rozenberg M J and Dobrosavljevic V 2015 *Phys. Rev. Lett.* **114** 246402
[18] Mikheev E, Hauser A J, Himmetoglu B, Moreno N E, Jannotti A, Van de walle C G *et al* 2015 *Sci. Adv.* **1** e1500797
[19] Weber M C, Guennou M, Dix N, Pesquera D, Sanchez F, Herranz G *et al* 2016 *Phys. Rev. B* **94** 014118
[20] Kumar Y, Bhatt H, Prajapat C L, Basu S and Singh S 2018 *J. Appl. Phys.* **124** 065302
[21] Gou G, Grinberg I, Rappe A M and Rondinelli J M 2011 *Phys. Rev. B* **84** 144101
[22] Chaban N, Weber M, Pignard S and Kreisel J 2010 *Appl. Phys.* **97** 031915
[23] Soni K, Yadav E, Harisankar S and Mavani K R 2020 *J. Phys. Chem. Solids* **141** 109398
[24] Zhao J, Guo H, He X, Zhang Q, Gu L, Li X *et al* 2018 *ACS Appl. Mater. Interfaces* **10** 10211
[25] Balkanski M, Wallis R F and Haro E 1983 *Phys. Rev. B* **28** 1928